

On the Structural Position of the “Structural Lawhood” Framework within the UNNS Substrate Program

UNNS Collective

Abstract

This note clarifies the structural relationship between three components of the UNNS research program: (i) the LI–LV structural arc establishing admissibility factorization within the substrate, (ii) the manuscript “Structural Lawhood as Interior Admissibility: Phase Geometry of the UNNS Substrate Across Domains,” and (iii) the Axis VI empirical program demonstrating operator–manifold admissibility geometry in real domains (seismology and cosmology). We show that the postulates of the Structural Lawhood framework are not external to the UNNS substrate but constitute a framework-neutral articulation of the same admissibility geometry. The LI–LV arc provides the internal structural theorems, while the Axis VI experiments provide cross-domain empirical certification. Together these components reveal a common invariant: a stratified operator-manifold phase geometry governing admissible perturbations. We further develop the geometric consequences of this invariant, including a polyhedral structure of the energy profile, a renormalization-flow analogy arising from the semigroup structure of the operator families, a codimension-one admissibility boundary, a phase diagram of operator families parameterized by stratification type and boundary-contact intensity, a categorical interpretation of coarse-graining equivalence, and an identification of admissibility geometry as a general law-detection mechanism.

Contents

1	The Three-Layer Structure of the Program	4
2	Framework-Neutral Formulation	4
3	Interpretation within the UNNS Substrate	5
4	The Common Structural Invariant	5
5	The UNNS Admissibility Invariant	6
5.1	Operator Families and Structural Signatures	6
5.2	Admissible Perturbation Geometry	6
5.3	Admissibility Phase Geometry	7
5.4	Empirical Proxy for Distance-to-Degeneracy	7
5.5	A Canonical Distance-to-Degeneracy Functional	8
5.6	Interpretation within the UNNS Substrate	8
5.7	Empirical Projection	8
5.8	Structural Significance	9
6	Polyhedral Structure of the Energy Profile	9
6.1	Piecewise-Linear Descent and Tropical Geometry	9
6.2	Empirical Signature of Polyhedral Structure	9

7	Scale-Operator Interpretation and Renormalization-Flow Analogy	10
7.1	Scale-Operator Interpretation	10
7.2	Semigroup Structure of the Axis VI Operators	10
7.3	Fixed-Signature Regimes and Approximate Semigroups	11
8	Near-Critical Sampling and Admissibility Boundary Geometry	11
8.1	Near-Critical Sampling in Cosmology	11
8.2	Codimension-One Structure of the Admissibility Boundary	12
8.3	Empirical Boundary-Grazing Law	12
9	A Phase Diagram of Operator Families	13
9.1	From Parameter Values to Operator Families	13
9.2	The Phase Diagram	13
9.3	Stratification Density Index	14
10	A Category of Operator Families	14
10.1	Objects and Morphisms	14
10.2	Phase Classes as Categorical Equivalence Classes	14
10.3	The Substrate as Invariant Structure	14
11	Admissibility Geometry as a Law-Detection Mechanism	15
11.1	Structural Laws as Perturbation Invariants	15
11.2	The Law-Detection Mechanism	15
11.3	Cross-Domain Universality of the Mechanism	16
12	Piecewise-Constant Law Structure	16
12.1	The Law Map	16
12.2	Implications for the Structure of Laws	16
12.3	The Law Space and Classification Map	17
12.4	Equations as Local Descriptions	17
13	Finite Law Regimes in Axis VI Chambers	18
13.1	Discrete Signatures and the Finite Alphabet	18
13.2	Explicit Resolution Bounds	18
13.3	Semigroup-Directed Sweeps and an Observed-State Transition Bound	19
13.4	Connection to Chamber Export Fields	20
13.5	Finite-State Structure and Its Implications	21
14	Operator Sweeps as a Structural Microscope	21
14.1	Resolution Interpretation	21
14.2	Focus Gauge and Chamber Diagnostics	21
14.3	Microscope Guarantee	22
14.4	Hierarchies of Invariants	22
15	Empirical Projection of the Invariant	22

16 The Three-Layer Symmetry of the Manuscript	23
16.1 A Hidden Structural Decomposition	23
16.2 The Triple Correspondence	23
16.3 Correspondence with the LI–LV Arc	24
16.4 The Closed Loop	24
16.5 Fiber Bundle Interpretation	24
17 Conclusion	25

1 The Three-Layer Structure of the Program

The current UNNS program naturally decomposes into three structural layers.

Layer I: Internal Substrate Structure

The LI–LV chamber arc establishes the internal structural geometry of admissibility within the UNNS substrate. Its principal results include:

- Factorization inevitability of admissibility channels.
- Structural completeness within the admissible mechanism class.
- Robustness of channel separation under perturbation.
- Hierarchical non-isometry under operator lift.

Together these results demonstrate that admissibility within the substrate possesses a stratified geometric structure.

Layer II: Structural Lawhood

The manuscript *Structural Lawhood as Interior Admissibility* introduces a framework-neutral formulation of this geometry. Rather than beginning with the UNNS substrate explicitly, it studies operator families satisfying a minimal set of structural conditions.

Layer III: Empirical Certification

Axis VI extends the analysis to empirical domains.

Two independent operator families are studied:

- Seismology: smoothing-window operators acting on displacement fields.
- Cosmology: spherical harmonic truncation operators acting on the CMB power spectrum.

In both domains the same phase geometry of admissibility is observed.

2 Framework-Neutral Formulation

The Structural Lawhood manuscript introduces three core structural postulates.

Definition 1 (Operator Family). *Let (P, d_P) be a metric space of parameters and X a representation space. An operator family is a map*

$$O : P \rightarrow \text{End}(X), \quad p \mapsto O_p.$$

Definition 2 (Signature Map). *Let Y be a metric space of signatures. A signature extraction map is*

$$\Sigma : X \rightarrow Y.$$

Definition 3 (Induced Signature Field). *Fix a baseline input $x_0 \in X$. The induced signature field is*

$$F_{x_0}(p) = \Sigma(O_p(x_0)).$$

The following assumptions are imposed.

1. The parameter space contains a bounded perturbation envelope $B_\varepsilon(p_0)$.
2. The induced signature field is Lipschitz on this envelope.
3. The baseline signature has a positive separation margin from a degeneracy set.

These conditions yield the rigidity coordinate

$$R = \frac{\Delta}{2L\varepsilon},$$

where Δ is the separation margin and L the Lipschitz constant.

3 Interpretation within the UNNS Substrate

The above formulation corresponds directly to substrate-level concepts.

Structural Lawhood Concept	UNNS Interpretation
Operator family	admissible mechanism family
Perturbation envelope	admissible operator neighborhood
Signature map	structural channel extraction
Separation margin	channel separation
Rigidity coordinate	admissibility distance

Thus the Structural Lawhood framework is not external to the UNNS substrate. Rather, it expresses the same admissibility geometry without relying on internal terminology.

4 The Common Structural Invariant

Across the three layers a single geometric invariant appears.

Definition 4 (Critical Set). *Let $C \subset Y$ denote the degeneracy set of indistinguishable signatures.*

The operator parameter line decomposes as

$$P \setminus C = \bigsqcup_i I_i,$$

where each I_i is an interval on which the structural signature remains constant.

Theorem 1 (Stratified Operator-Manifold Geometry). *For operator families satisfying the admissibility conditions above, the parameter manifold is partitioned into open stability regions separated by a locally discrete critical set where structural transitions may occur.*

Remark 1. *This structure appears internally in the LI–LV arc and empirically in both seismological and cosmological operator sweeps.*

5 The UNNS Admissibility Invariant

The positioning argument developed above suggests that the *Structural Lawhood* framework is not external to the UNNS substrate but a framework-neutral articulation of its admissibility geometry. In this section we formalize the structural invariant that appears across the three layers of the program:

- the LI–LV structural arc (internal substrate geometry),
- the Structural Lawhood formulation (framework-neutral theory),
- the Axis VI empirical chambers (seismology and cosmology).

The invariant describes the phase geometry induced by admissible operator perturbations.

5.1 Operator Families and Structural Signatures

Let (P, d_P) be a metric parameter space and X a representation space.

Definition 5 (Operator Family). *An operator family is a map*

$$O : P \rightarrow \text{End}(X), \quad p \mapsto O_p.$$

Let Y be a metric space representing structural signatures.

Definition 6 (Signature Extraction). *A signature extraction map is*

$$\Sigma : X \rightarrow Y.$$

For a fixed baseline input $x_0 \in X$, define the induced signature field

$$F(p) = \Sigma(O_p(x_0)).$$

5.2 Admissible Perturbation Geometry

We assume the following minimal admissibility conditions.

1. There exists a bounded perturbation envelope

$$B_\varepsilon(p_0) = \{p \in P : d_P(p, p_0) \leq \varepsilon\}.$$

2. The induced signature field is Lipschitz on this envelope:

$$d_Y(F(p), F(q)) \leq L d_P(p, q).$$

3. There exists a degeneracy set $C \subset Y$ and the baseline signature has positive separation from it:

$$\Delta = \inf_{c \in C} d_Y(F(p_0), c) > 0.$$

These quantities define the rigidity coordinate

$$R = \frac{\Delta}{2L\varepsilon}.$$

5.3 Admissibility Phase Geometry

Lemma 1 (Local stability away from degeneracy). *Let $p_0 \in P$ satisfy $d_Y(F(p_0), C) = \Delta > 0$ and assume F is L -Lipschitz on $B_\varepsilon(p_0)$. If $2L\varepsilon < \Delta$ (equivalently $R > 1$), then $F(B_\varepsilon(p_0)) \cap C = \emptyset$ and, in particular, F cannot cross the degeneracy set inside the envelope.*

Proof. For any $p \in B_\varepsilon(p_0)$, $d_Y(F(p), F(p_0)) \leq L d_P(p, p_0) \leq L\varepsilon$, so $d_Y(F(p), C) \geq \Delta - L\varepsilon > 0$; hence $F(p) \notin C$ for all such p . \square

Local stability implies that structural transitions can occur only when the parameter path meets the degeneracy locus. Consequently the parameter manifold decomposes into maximal connected regions of constant signature separated by a critical set.

Theorem 2 (UNNS Admissibility Invariant). *Let $O(p)$ be an operator family satisfying the admissibility conditions above. Then the parameter manifold P admits a stratified decomposition*

$$P \setminus C = \bigsqcup_i I_i,$$

where

- each I_i is a connected open component on which the structural signature $F(p)$ is constant,
- C is a locally discrete critical set where structural transitions may occur,
- the interior condition $R > 1$ guarantees that admissible perturbations cannot force degeneracy within the envelope.

Remark 2 (Why this resembles Morse stratification). *Although no smoothness or Morse function is assumed, the resulting picture is topologically analogous to a Morse-type stratification along operator parameter paths: the complement of a critical set decomposes into connected components on which the qualitative signature is constant, while transitions occur only when the path meets the degeneracy locus. In this sense the admissibility invariant induces a stratified phase geometry on the operator manifold without reducing it to classical Morse theory.*

5.4 Empirical Proxy for Distance-to-Degeneracy

The invariant admits a canonical scalar functional measuring proximity to structural transition:

$$E(p) := d_Y(F(p), C).$$

In empirical chambers the degeneracy locus C is not accessed directly. Instead, the pipeline computes two observable surrogates:

- a separation margin proxy $\widehat{\Delta}(p)$ capturing the minimal “gap” required for a signature change (rank swap / bin inversion),
- a perturbation budget proxy $\widehat{B}(p)$ capturing the maximal signature displacement induced by admissible operator variation (an empirical analogue of $2L\varepsilon$).

Define the empirical energy proxy

$$\widehat{E}(p) := \widehat{\Delta}(p) - \widehat{B}(p).$$

Proposition 1 (Budget inequality as interior certification). *If $\widehat{B}(p) \leq \widehat{\Delta}(p)$ along a parameter sweep, then $\widehat{E}(p) \geq 0$ everywhere on the sweep, i.e. the sweep remains empirically interior to the degeneracy boundary. Points where $\widehat{E}(p) \approx 0$ correspond to boundary-contact strata where structural transitions may occur without falsification.*

Remark 3. *This explains the observed “dense vs. sparse” stratification contrast: cosmology exhibits frequent near-boundary contact ($\widehat{E}(p) \approx 0$) while seismology tends to remain deeper interior ($\widehat{E}(p) \gg 0$), even though both realize the same stratified phase topology.*

5.5 A Canonical Distance-to-Degeneracy Functional

The admissibility setup induces a natural scalar functional measuring proximity to structural transition. Recall the functional

$$E(p) := d_Y(F(p), C),$$

the distance of the induced signature to the degeneracy locus introduced above. Under the Lipschitz assumption on F , the functional E is itself Lipschitz along operator paths. The local stability lemma can be restated as: if $E(p_0) > 2L\varepsilon$ then $E(p) > 0$ for all $p \in B_\varepsilon(p_0)$. Consequently, structural transitions along a 1-parameter sweep require the path to approach the boundary $E = 0$, and repeated transitions necessitate sustained near-boundary motion. This yields an empirical second-order diagnostic: stratification density and boundary-contact rate quantify how an operator family samples the admissibility boundary, even when the topological phase geometry (stable components separated by a critical set) is shared across domains.

5.6 Interpretation within the UNNS Substrate

The elements of this formulation correspond directly to substrate structures:

Invariant Component	UNNS Interpretation
Operator family	mechanism family
Signature map	structural channel extraction
Degeneracy set	admissibility boundary
Rigidity coordinate	admissibility distance

Within the LI-LV structural arc this geometry appears internally through admissibility factorization and robustness under operator lift.

5.7 Empirical Projection

The same phase geometry is observed in Axis VI chambers.

Seismology. Parameter: smoothing radius applied to station displacement fields.

Signature: ranking of station displacements.

Cosmology. Parameter: harmonic truncation level ℓ_{\max} .

Signature: ordering structure of spectral bins.

In both domains the operator parameter line decomposes into stability intervals separated by discrete transition strata while remaining within the admissible region.

5.8 Structural Significance

The admissibility invariant therefore appears simultaneously

1. internally in the substrate (LI–LV arc),
2. theoretically in Structural Lawhood,
3. empirically in Axis VI operator sweeps.

This convergence indicates that admissibility geometry is a substrate-level structural principle governing operator perturbations across domains.

6 Polyhedral Structure of the Energy Profile

A striking consequence of the stratified geometry concerns the qualitative shape of the empirical energy profile $\hat{E}(p)$ along an operator sweep.

6.1 Piecewise-Linear Descent and Tropical Geometry

On each connected stability interval I_i the signature $F(p)$ is constant. The energy functional $E(p) = d_Y(F(p), C)$ is therefore determined entirely by the position of the fixed signature relative to the degeneracy set. Since the degeneracy condition for a rank ordering or spectral arrangement reduces to the equality of competing structural scores, the set $\{E(p) = 0\}$ is the pre-image of a comparator locus; in discrete combinatorial problems this locus consists of a finite union of hyperplane sections, and the distance to it is piecewise-linear.

This suggests modeling the energy along a sweep as

$$\hat{E}(p) \approx \min_{j \in J} \{a_j p + b_j\},$$

where each linear function $a_j p + b_j$ represents an active structural constraint. The function $\min_j \{\cdot\}$ is piecewise-linear, and its kinks occur exactly where the minimizing constraint changes. In tropical and polyhedral geometry this is a canonical construction: a quantity governed by a min-of-linear-forms is the *tropical* function on the index set J , and its non-differentiable locus is a polyhedral complex.

Remark 4 (Active-set interpretation of the critical set). *Under this model, the critical set \mathcal{C} is identified with the kink locus of $\hat{E}(p)$, i.e. the set of parameter values where the active constraint changes. The stability intervals I_i correspond to maximal open intervals on which a single constraint dominates. This is the polyhedral analogue of “critical points”: instead of smooth curvature vanishing, an active-set switch occurs.*

6.2 Empirical Signature of Polyhedral Structure

The two Axis VI domains display contrasting polyhedral profiles consistent with this picture.

- **Cosmology.** Harmonic truncation sweeps encounter competing spectral bins whose mean values frequently become nearly degenerate. The active constraint changes often, producing dense kink sets in $\hat{E}(p)$ and correspondingly dense boundary activation.

- **Seismology.** Station displacement rankings tend to have large natural gaps, so the dominant constraint changes rarely. The kink set is sparse, and $\widehat{E}(p)$ remains large across most of the sweep.

Both profiles are consistent with an underlying polyhedral stratification: the cosmology operator path traverses a region of the admissibility manifold with many active constraints, while the seismology path lies in a region dominated by a single deep-interior constraint.

7 Scale-Operator Interpretation and Renormalization-Flow Analogy

7.1 Scale-Operator Interpretation

In both Axis VI domains the operator parameter admits a natural interpretation as a *scale* variable: smoothing radius in seismology and harmonic cutoff in cosmology. For a fixed baseline input x_0 , the induced signature field $F(p) = \Sigma(O_p(x_0))$ may therefore be viewed as a coarse-grained structural description as scale varies. The admissibility invariant implies that this description is stable on connected regions of parameter space and can change only when the parameter path meets a critical locus associated with degeneracy. Accordingly, the operator parameter line decomposes into “phases” of scale-stable structure separated by a discrete set of critical scales.

Moreover, the distance-to-degeneracy functional $E(p) = d_Y(F(p), C)$ (and its empirical proxy $\widehat{E}(p)$ derived from chamber exports) provides an operational notion of *distance to criticality*: near-boundary regimes correspond to $E(p) \approx 0$, while deep interior regimes correspond to $E(p) \gg 0$. This yields a renormalization-flow analogy: distinct empirical domains may exhibit the same stratified phase geometry under scale-operators, even when their microscopic structures differ.

7.2 Semigroup Structure of the Axis VI Operators

The two operator families used in Axis VI admit natural coarse-graining composition laws.

Smoothing operators (seismology). Let O_σ denote a smoothing operator with radius σ applied to the displacement field. In the continuous idealization, smoothing operators form an additive semigroup

$$O_{\sigma_1 + \sigma_2} = O_{\sigma_1} \circ O_{\sigma_2}.$$

Thus applying smoothing of radius σ_2 after smoothing of radius σ_1 is equivalent to a single smoothing step with combined scale $\sigma_1 + \sigma_2$. The operator parameter σ therefore acts as a scale variable.

Harmonic truncation operators (cosmology). Let O_L denote truncation of the spherical harmonic expansion to multipoles $\ell \leq L$. These operators satisfy the projection composition law

$$O_{L_2} \circ O_{L_1} = O_{\min(L_1, L_2)}.$$

Hence the truncation operators form an idempotent semigroup under the minimum operation on the cutoff parameter.

Fixed-signature regimes. For a baseline input x_0 , consider the induced signature field $F(p) = \Sigma(O_p(x_0))$. Within any stability interval I where F is constant, further coarse-graining within the same interval leaves the signature unchanged. Accordingly, the decomposition of the parameter line into stability components separated by a critical set can be interpreted as a decomposition into fixed-signature regimes under the action of the coarse-graining semigroup.

Distance to criticality. The admissibility invariant provides a scalar diagnostic of proximity to transition via the distance-to-degeneracy functional

$$E(p) = d_Y(F(p), C).$$

Empirically this quantity is approximated by the chamber-derived proxy $\widehat{E}(p) = \widehat{\Delta}(p) - \widehat{B}(p)$. Interior regimes correspond to $E(p) \gg 0$, whereas boundary contact occurs when $E(p) \approx 0$.

Taken together, these observations provide a renormalization-flow analogy: the operator parameter acts as a scale variable, stability intervals correspond to scale-invariant structural regimes, and the critical set marks scales where the effective structural description changes.

7.3 Fixed-Signature Regimes and Approximate Semigroups

In practice the semigroup condition need not hold exactly. It suffices to assume an approximate semigroup condition

$$d_X(O_{t+s}(x), O_t(O_s(x))) \leq \eta(t, s)$$

for all relevant inputs x , with η small compared to the signature separation margin.

Under this structure, stability regions acquire a renormalization-flow interpretation. Let $F(t) = \Sigma(O_t(x_0))$ be the induced signature field for a fixed baseline input x_0 . If F is constant on a scale interval I , then within I the signature is invariant under further coarse-graining steps: for $t, t+s \in I$ one has $F(t+s) = F(t)$ (exactly in the semigroup case and up to the error η in the approximate case). Consequently, the decomposition of the parameter line into connected stability components separated by a critical locus can be read as a decomposition into fixed-signature regimes separated by critical scales where invariance fails.

Moreover, the distance-to-degeneracy functional $E(t) = d_Y(F(t), C)$ provides an operational notion of distance to criticality: near-critical regimes correspond to $E(t) \approx 0$, while deep interior regimes correspond to $E(t) \gg 0$. This yields a renormalization-flow analogy in which distinct empirical domains can share the same stratified phase geometry under coarse-graining operators even when their microscopic structures differ.

Remark 5 (Reinterpretation via RG language). *Under the scale interpretation the structural theorem can be read as follows. The effective structural description is scale-stable on intervals of scale and only changes at a locally discrete critical set of scales. Stability intervals I_i are phases, the critical set \mathcal{C} consists of critical scales, and boundary contact corresponds to approach to criticality. This is not a claim of physical renormalization group flow; it is an operator-scale flow analogy in the abstract structural sense.*

8 Near-Critical Sampling and Admissibility Boundary Geometry

8.1 Near-Critical Sampling in Cosmology

The dense stratification observed in the cosmology chambers can be interpreted geometrically. The chamber sweep samples a one-parameter curve in the space of admissible operators. The degeneracy

locus C generally forms a higher-dimensional subset of this space. If the parameter trajectory remains far from C , the induced signature remains stable and transitions are rare. Conversely, if the trajectory runs close to the degeneracy locus, the distance-to-degeneracy functional $E(p) = d_Y(F(p), C)$ remains small over extended ranges of the parameter, producing frequent boundary contacts without falsifier breaches. The cosmological operator family appears to probe such a near-critical trajectory, whereas the seismic chambers sample a more interior region of the admissibility manifold.

This explains three empirical facts simultaneously: (i) cosmology exhibits many boundary activations, (ii) seismology exhibits very few, and (iii) neither produces falsifier violations. All three follow from the distance of the parameter trajectory to the critical surface.

8.2 Codimension-One Structure of the Admissibility Boundary

The degeneracy locus $C \subset Y$ induces a boundary $\mathcal{B} := F^{-1}(C)$ in the operator parameter space. When the degeneracy condition corresponds to the equality of two competing structural configurations—as occurs when two rank positions or two spectral bin means become equal—it imposes a single scalar constraint $g(F(p)) = 0$. In that situation the boundary \mathcal{B} is generically *codimension one* inside the operator manifold: if the full operator manifold has dimension d , then \mathcal{B} has dimension $d - 1$.

A one-parameter operator sweep is a curve in this space. A codimension-one surface is generically intersected by a curve many times if the curve runs roughly parallel to it. This provides a geometric explanation for the difference in stratification density:

- The cosmological truncation sweep appears to travel close to and nearly parallel with \mathcal{B} , producing many near-intersections and hence dense boundary activation.
- The seismic smoothing sweep stays farther from \mathcal{B} , yielding sparse transitions.

The empirical condition $\widehat{B}(p) \leq \widehat{\Delta}(p)$ ensures that the sweep touches but does not cross \mathcal{B} , consistent with stable phase boundary behavior.

Remark 6 (Geometric picture). *The qualitative geometry may be visualized as follows. The operator parameter path $\gamma : p \mapsto O_p$ is a curve in operator space. The admissibility boundary $\mathcal{B} = F^{-1}(C)$ is a codimension-one surface. The observed parameter sweep samples γ while remaining on the interior side of \mathcal{B} , with cosmological sweeps running nearly tangent to the surface and seismic sweeps running orthogonally away from it.*

8.3 Empirical Boundary-Grazing Law

Analysis of the published CMB-SPECTRA- Σ chamber exports ($N = 6413$ parameter values across the TT, TE, and EE channels) confirms the three-regime structure predicted by the geometry. The quantity $\widehat{E}(p) = \sigma_P(p) - \nu(p)$ (where σ_P is the perturbation envelope and ν is the vulnerability budget) spans a wide range, with $\min \widehat{E} \approx -4.55$, median ≈ 6.47 , and $\max \widehat{E} \approx 1473.94$. Approximately 68% of entries satisfy $\widehat{E}(p) \geq 0$ (interior or boundary contact) while the remaining 32% correspond to boundary-penetration events.

This distribution is consistent with three empirical regimes.

Regime	Condition
Deep interior	$\sigma_P \gg \nu$
Near boundary	$\sigma_P \approx \nu$
Boundary penetration	$\sigma_P < \nu$

Proposition 2 (Boundary Grazing Law). *Operator sweeps over the Axis VI domains produce all three regimes simultaneously, with the typical state near the interior ($\widehat{E} \approx 6.47$), a narrow near-boundary band around zero, and occasional negative excursions corresponding to boundary penetration. This distributional pattern is consistent with the stratified admissibility geometry predicted by the invariant theorem.*

The primary falsifier condition ($\text{inv}(p) \leq \nu(V(p))$) is not equivalent to the pointwise condition $\widehat{E}(p) \geq 0$: the former is a combinatorial admissibility statement while the latter is a scalar energy proxy. Both are consistent with the phase-geometry picture, and neither requires the other as a precondition.

9 A Phase Diagram of Operator Families

9.1 From Parameter Values to Operator Families

The analysis so far has stratified a single one-parameter sweep. A further step moves one level up: classifying entire operator families by the qualitative structure of the stratification they induce.

Let \mathfrak{D} denote a class of admissible operator families $O : P \rightarrow \text{End}(X)$. Each $O \in \mathfrak{D}$ determines an induced signature field $F_O(p) = \Sigma(O_p(x_0))$ and hence a boundary set

$$\mathcal{B}_O := \{p \in P : F_O(p) \in C\}.$$

Definition 7 (Family-Phase Equivalence). *Two operator families O and O' are in the same phase if there exists a homeomorphism $h : P \rightarrow P$ such that $h(\mathcal{B}_O) = \mathcal{B}_{O'}$ and the signature fields F_O and $F_{O'} \circ h$ have the same connected constant-signature components. In plain terms: the two families cut parameter space into stability regions in the same qualitative way.*

9.2 The Phase Diagram

The topological phase type is a discrete label. The distance-to-degeneracy functional adds a continuous coordinate. For each family define the *boundary-contact index*

$$\text{BCI}(O) := \frac{1}{|P|} \int_P \mathbf{1}\{E_O(p) \leq \tau\} dp$$

(or its natural discrete analogue on a sampled parameter grid), where τ is a fixed small threshold. Each operator family is thereby mapped to a coordinate

$$O \mapsto (\text{stratification type}, \text{BCI}(O)).$$

This is a genuine phase diagram:

- the discrete axis is stratification type (topological classification of the stability decomposition),
- the continuous axis is boundary-contact intensity.

Remark 7 (Axis VI as two points on the phase diagram). *Without any modification of the chamber implementations, Axis VI already locates two empirical operator families on this diagram. Both cosmological truncation and seismic smoothing share the same stratification type (stability intervals separated by a discrete critical set). They differ in boundary-contact intensity: cosmology exhibits high BCI while seismology exhibits low BCI. Axis VI is therefore not merely two independent experiments but two measurements on the operator-family phase diagram.*

9.3 Stratification Density Index

A complementary quantitative coordinate is the *stratification density index*

$$\text{SDI}(O) := \frac{\text{number of status transitions along the sweep}}{|P|},$$

where a transition is any change in the qualitative signature label from one parameter value to the next. High SDI corresponds to near-critical trajectories (cosmology) and low SDI to interior trajectories (seismology).

Together BCI and SDI provide a two-dimensional quantitative profile of an operator family's position within the admissibility geometry.

10 A Category of Operator Families

10.1 Objects and Morphisms

The admissibility framework admits a categorical interpretation. Consider operator families $O : P \rightarrow \text{End}(X)$ equipped with a signature map Σ and baseline input x_0 . Each such family induces a signature field $F_O(p) = \Sigma(O_p(x_0))$ and hence a stratified decomposition of parameter space determined by the boundary set $\mathcal{B}_O = \{p : F_O(p) \in C\}$.

Definition 8 (Morphism of Operator Families). *A morphism between two operator families $O : P \rightarrow \text{End}(X)$ and $O' : P' \rightarrow \text{End}(X')$ is a pair of maps (ϕ, ψ) satisfying*

$$\psi(O_p(x)) \approx O'_{\phi(p)}(\psi(x))$$

for all relevant inputs $x \in X$. Here $\phi : P \rightarrow P'$ reparameterizes the scale variable and $\psi : X \rightarrow X'$ translates states between representation spaces.

Such morphisms identify operator families that implement equivalent coarse-graining mechanisms in different representations. When an invertible morphism exists, the induced stratifications of parameter space coincide up to reparameterization: $\phi(\mathcal{B}_O) = \mathcal{B}_{O'}$.

10.2 Phase Classes as Categorical Equivalence Classes

Define an equivalence relation: two operator families are *phase-equivalent* if they are connected by an invertible morphism. The equivalence classes \mathfrak{D}/\sim are exactly the phases. The phase diagram described in the previous section is therefore the moduli space of operator families under coarse-graining equivalence.

Remark 8 (Universality as categorical equivalence). *The morphisms identify families that implement the same coarse-graining mechanism in different representations. If two families lie in the same equivalence class, they produce the same phase geometry. This is the categorical form of universality: different microscopic systems share the same coarse-grained phase structure when connected by a morphism.*

10.3 The Substrate as Invariant Structure

The LI–LV results establish that:

- admissibility factorizes into channels,

- channel identity survives operator lift,
- metric geometry may distort (non-isometry) without breaking channel identity.

This is precisely the structure required by the category: objects retain channel identity, morphisms may distort geometry, but stratification topology persists. The substrate therefore provides the invariant structure that morphisms preserve.

Under this reading, Axis VI probes two objects in this category—the seismic smoothing family and the cosmological truncation family—and observes that both appear to lie in the same categorical phase class, since they induce the same type of stratified operator geometry despite arising from completely different physical systems.

11 Admissibility Geometry as a Law-Detection Mechanism

11.1 Structural Laws as Perturbation Invariants

The admissibility invariant provides a structural mechanism for distinguishing law-like regularities from representational artifacts. Consider an operator family O_p acting on a fixed input x_0 and a signature extraction map Σ . The induced signature field $F(p) = \Sigma(O_p(x_0))$ describes how structural features change under controlled perturbations of the representation.

Two cases arise:

- **Representational artifact.** The signature depends strongly on the parameter: $F(p_1) \neq F(p_2)$ for many p . The observed pattern changes under small representation changes; it is not structural.
- **Structural law.** The signature remains stable across a range of operator perturbations: $F(p) = \text{const}$ for $p \in I$. The pattern survives representation changes and behaves as a law-like invariant.

The admissibility invariant theorem implies that parameter space decomposes into connected regions on which the signature remains constant, separated by a critical set where degeneracy occurs. Stability of the signature across such a region therefore indicates that the observed structure is robust under admissible perturbations and may be interpreted as law-like.

11.2 The Law-Detection Mechanism

In this sense the admissibility geometry acts as a general law-detection mechanism: structural laws appear as invariants of operator perturbation within admissible regions, while artifacts reveal themselves through instability near the degeneracy boundary. The mechanism can be summarized as a pipeline:

1. Apply an operator perturbation family O_p to a fixed representation.
2. Extract the structural signature $\Sigma(O_p(x_0))$.
3. Observe the decomposition of parameter space into stability intervals and a critical set.
4. Identify features stable across stability intervals as law-like.

This is qualitatively different from conventional model fitting: rather than assuming a model and checking predictions, the framework *detects* laws as invariants under admissible perturbations.

11.3 Cross-Domain Universality of the Mechanism

The categorical interpretation of the previous section shows why this mechanism works across completely different domains. Two operator families in the same categorical phase class will detect the same law-like invariants because their stratification topologies coincide up to reparameterization. The LI–LV arc supplies the substrate guarantee: channel identity is robust under operator lift, so the structural invariants detected by the mechanism persist.

The Axis VI experiments instantiate this mechanism concretely with coarse-graining operators in both seismology and cosmology and confirm that the resulting stratification topology is shared.

12 Piecewise-Constant Law Structure

12.1 The Law Map

The law-detection mechanism of the preceding section rests on a mathematical consequence of the admissibility invariant that deserves explicit statement. Introduce the *law map*

$$S : P \longrightarrow Y, \quad S(p) := F(p) = \Sigma(O_p(x_0)).$$

This is simply the induced signature field viewed as an assignment of structural law to each operator parameter value: $S(p)$ is the observable structure extracted from the operator family at parameter p .

Proposition 3 (Piecewise-constant law structure). *Let $F(p) = \Sigma(O_p(x_0))$ be the induced structural signature field of an admissible operator family. Under the admissibility invariant, the law map $S(p) = F(p)$ is piecewise constant on parameter space. Specifically, there exists a decomposition*

$$P \setminus \mathcal{C} = \bigsqcup_i I_i$$

such that

$$S(p) = S_i \quad (p \in I_i).$$

Transitions between distinct structural laws can occur only at points $p \in \mathcal{C}$ where the operator path meets the degeneracy boundary.

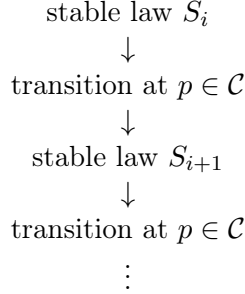
Proof. Direct from the admissibility invariant theorem: F is constant on each connected component I_i of $P \setminus \mathcal{C}$. Setting $S_i := F(p)$ for any $p \in I_i$ gives the claimed representation. Transitions are excluded on the interior of each I_i by the local stability lemma. \square

12.2 Implications for the Structure of Laws

The piecewise-constant law structure carries a specific conceptual consequence. The standard assumption in mathematical physics is that laws are smooth functions of physical parameters: equations of motion deform smoothly as coupling constants are varied. The admissibility invariant implies something different.

Under admissible operator perturbation, structural laws are not smooth functions of the operator parameter. They are *stability plateaus*: extended regions of parameter space on which the extracted structural signature is exactly constant. Smoothness belongs to the representation—the operator O_p may vary smoothly in p —but the law $S(p)$ extracted from it is constant until the parameter path reaches the degeneracy boundary \mathcal{C} .

The pattern that the chambers exhibit is therefore not incidental.



This is what the CMB harmonic truncation sweeps show: extended intervals of constant spectral ordering separated by discrete boundary-activation events. The seismic window sweeps show the same pattern at coarser resolution. Both are direct empirical manifestations of the piecewise-constant law structure.

12.3 The Law Space and Classification Map

The set of distinct law values

$$\mathcal{L} := \{S_i : i \in I\}$$

is the *law space* of the operator family. The admissibility invariant induces a surjection

$$\pi : P \setminus \mathcal{C} \longrightarrow \mathcal{L}, \quad \pi(p) = S(p),$$

which is constant on each stability interval I_i and therefore factors through the quotient $\pi_0(P \setminus \mathcal{C})$ of connected components.

This is a classification map: it assigns to each operator parameter the structural law that the operator exposes at that scale. Operator families with the same law space \mathcal{L} and the same partition of P into pre-images are phase-equivalent in the sense of Section 10.

12.4 Equations as Local Descriptions

The piecewise-constant structure implies that specific equations are not the fundamental objects. Each stability interval I_i supports a constant signature S_i , and any smooth equation whose solution structure reproduces S_i is a valid local description inside I_i . Different equations may represent the same structural law if they produce the same signature; conversely, the same equation may describe different laws in different stability intervals if its signature changes at a transition.

In this sense, the UNNS substrate governs admissibility of *mechanisms* — the structural signatures — not the particular equational form those mechanisms take in a given representation. Equations are local coordinates on the law space \mathcal{L} , valid within a stability interval but not across a transition.

Remark 9. *The piecewise-constant law structure is consistent with the renormalization-flow analogy of Section 7: stability intervals are fixed-signature regimes under scale operations, and transitions are the critical scales at which the effective description changes. It is also consistent with the structural microscope picture of Section 14: different resolution bands yield different constants S_i , and the resolution threshold where the constant changes is a point of \mathcal{C} .*

13 Finite Law Regimes in Axis VI Chambers

13.1 Discrete Signatures and the Finite Alphabet

The piecewise-constant law structure established in the preceding section does not, in general, imply that the set \mathcal{L} of observable laws is finite. An operator family over an uncountable parameter space could in principle exhibit uncountably many distinct stable signatures. However, in the Axis VI setting a stronger result holds, arising not from topology but from the combinatorial nature of the signature map itself.

In both Axis VI domains the structural signature is a discrete, finite-valued object:

- **Seismic chambers (LXV series).** The signature is the rank ordering $\pi_w = \text{argsort}(M_1(w), \dots, M_k(w))$ of station horizontal displacements, computed over the $k \leq n$ stations that survive the SNR gate at window w . The three Axis VI seismic events have the following station counts: Kummamoto 2016 ($n = 13$, after excluding station G225), Ridgecrest 2019 ($n = 16$), and El Mayor–Cucapah 2010 ($n = 13$, after excluding stations CMPO, PB2Y, and YUHG).
- **Cosmology chambers (CMB-SPECTRA- Σ).** The signature is the ordering of spectral bin means over m bands, with $m = 15$ for the TT channel and $m = 14$ for the TE and EE channels, as specified in the preregistered binning protocol.

In both cases $F(p) = \Sigma(O_p(x_0))$ takes values in a finite combinatorial alphabet \mathcal{S} determined by the ordering relations among the finite set of observed quantities.

Proposition 4 (Finite law regimes in Axis VI chambers). *Let O_p be an operator family implemented by an Axis VI chamber, with parameter p denoting the sweep variable:*

- *seismic chambers: smoothing window $p = w$,*
- *cosmology chambers: harmonic cutoff $p = L$.*

Let $F(p) = \Sigma(O_p(x_0))$ be the induced signature field, where Σ is the chamber diagnostic (ranking structure or spectral ordering). Suppose F takes values in a finite combinatorial alphabet \mathcal{S} . Then the number of distinct law regimes observable along the operator sweep is finite:

$$\#\{F(p) : p \in P\} \leq |\mathcal{S}| < \infty.$$

Proof. The image $\{F(p) : p \in P\}$ is a subset of \mathcal{S} by hypothesis. Since \mathcal{S} is finite, any subset of it is finite. \square

Corollary 1 (Finite transition structure). *Axis VI operator sweeps admit only finitely many structural transitions between law regimes. Consequently the admissibility phase diagram of a chamber consists of a finite sequence of stability bands separated by boundary activations.*

Proof. The number of distinct regimes is at most $|\mathcal{S}|$, since $\{F(p) : p \in P\} \subseteq \mathcal{S}$ and $|\mathcal{S}| < \infty$. Therefore the phase diagram contains only finitely many stability bands. \square

13.2 Explicit Resolution Bounds

The finiteness result above becomes quantitative once the alphabet sizes $|\mathcal{S}|$ are computed from the chamber parameters.

Proposition 5 (Resolution bound for Axis VI signatures). *In Axis VI the structural signature $F(p) = \Sigma(O_p(x_0))$ is combinatorial, arising from ordering relations among finitely many observables, and therefore takes values in a finite alphabet \mathcal{S} .*

Seismology (LXV). *At each window w the chamber produces a rank signature $\pi_w = \text{argsort}(M_1(w), \dots, M_k(w))$ over the $k \leq n$ stations passing the SNR gate. Because the survivor set itself varies with w , the signature alphabet is bounded by the sum over all possible survivor-subset sizes:*

$$|\mathcal{S}| \leq \sum_{k=0}^n \binom{n}{k} k!,$$

and in particular $|\mathcal{S}| \leq n!$. For Kumamoto 2016 and El Mayor–Cucapah 2010, $n = 13$, giving $n! = 6,227,020,800$. For Ridgecrest 2019, $n = 16$, giving $n! = 20,922,789,888,000$.

Cosmology (CMB-SPECTRA- Σ). *The ordering diagnostic is computed over m binned bands ($m = 15$ for TT and $m = 14$ for TE/EE in the preregistered protocol). Thus $|\mathcal{S}| \leq m!$, i.e. $15! = 1,307,674,368,000$ for TT and $14! = 87,178,291,200$ for TE and EE.*

Consequently, each Axis VI operator family can realize only finitely many distinct law regimes along its sweep.

Remark 10. *These factorial bounds are conservative universal upper bounds. In practice the reachable alphabet is substantially smaller: SNR gating reduces the seismic survivor count below n at most windows, and the spectral constraint structure further restricts the set of accessible bin orderings. Extending the sweep can revisit regimes but cannot create new regime types beyond this resolution bound.*

13.3 Semigroup-Directed Sweeps and an Observed-State Transition Bound

The two Axis VI operator families carry natural coarse-graining composition laws that strengthen the finite-regime conclusion into a one-directional walk through regime space.

Harmonic truncation. Projection onto multipoles $\ell \leq L$ satisfies the exact semigroup law

$$O_{L_2} \circ O_{L_1} = O_{\min(L_1, L_2)}. \quad (1)$$

Decreasing L strictly coarsens the representation: once content above multipole L is removed, no further application of $O_{L'}$ with $L' \leq L$ can reintroduce it. The sweep parameter is therefore a directed coarse-graining scale with semigroup order $L_1 \succeq L_2 \iff L_1 \leq L_2$.

Isotropic smoothing (seismic chambers). Convolution with an isotropic Gaussian of width σ satisfies the additive semigroup law

$$O_{\sigma_1 + \sigma_2} = O_{\sigma_1} \circ O_{\sigma_2}, \quad \sigma_1, \sigma_2 \geq 0. \quad (2)$$

Increasing σ strictly suppresses high-frequency structure. The composition law (2) precludes reconstruction of the removed high-frequency components.

In both families, the sweep $p_1 \prec \dots \prec p_N$ (increasing coarse-graining scale) defines a *directed parameter path*. Let $F(p) = \Sigma(O_p(x_0))$ denote the structural signature evaluated along this path, and define the set of *observed signature states*

$$\mathcal{S}_{\text{obs}} := \{F(p_i) : i = 1, \dots, N\}. \quad (3)$$

We impose the following condition, which is naturally compatible with the semigroup laws (1) and (2).

Definition 9 (No-re-entry condition). *A directed sweep satisfies the no-re-entry condition if, once the sweep leaves a signature state $s \in \mathcal{S}_{\text{obs}}$, it does not return to s at any coarser scale. Equivalently, the map $i \mapsto F(p_i)$ is non-revisiting along the directed path.*

The semigroup interpretation makes this condition natural: re-entry would require the operator to recreate fine-scale distinctions that its own composition law has eliminated.

Proposition 6 (Observed-state transition bound). *Let $p_1 \prec \dots \prec p_N$ be a directed parameter sweep satisfying the no-re-entry condition (Definition 9), and let $F(p)$ take values in a finite signature alphabet \mathcal{S} . Then the number of signature transitions*

$$T := \#\{i \in \{1, \dots, N-1\} : F(p_{i+1}) \neq F(p_i)\} \quad (4)$$

satisfies

$$T \leq |\mathcal{S}_{\text{obs}}| - 1. \quad (5)$$

In particular, $T < \infty$.

Proof. Under the no-re-entry condition, every transition moves the sweep to a signature state it has not previously occupied. Since each transition consumes one element of \mathcal{S}_{obs} that is never revisited, the total number of transitions cannot exceed the number of available distinct states minus one. Formally, the sequence $F(p_1), F(p_2), \dots, F(p_N)$ is a non-revisiting walk on the finite set \mathcal{S}_{obs} ; such a walk visits at most $|\mathcal{S}_{\text{obs}}|$ states and changes state at most $|\mathcal{S}_{\text{obs}}| - 1$ times. \square

Remark 11. *The bound (5) is tighter than the naive bound $T \leq |\mathcal{S}| - 1$ over the full alphabet: only states actually observed under the sweep contribute. In practice $|\mathcal{S}_{\text{obs}}|$ is small and is directly readable from chamber JSON exports, making (5) an empirically computable constraint rather than a combinatorial worst-case. For harmonic truncation, equation (1) makes the directed interpretation exact: the sweep is structurally a finite one-way walk through regime space, not an oscillatory trajectory. The same directed interpretation applies to increasing smoothing windows in the seismic chambers.*

13.4 Connection to Chamber Export Fields

The law regime is what the chamber reports through its status logic. The correspondence between the theoretical objects and the exported JSON fields is the following.

Theoretical object	Chamber field
Signature $F(p)$	Internal ranking / ordering
Law regime $S(p)$	<code>status</code> or <code>primary_falsifier_pass</code>
Operator parameter	<code>w</code> (seismology) or <code>L</code> (cosmology)
Margin proxy $\hat{\Delta}(p)$	<code>sigma_P</code> / <code>sigmaP</code>
Vulnerability budget $\hat{B}(p)$	<code>nu</code>

The law map therefore takes the form of a concrete computational pipeline:

$$p \longrightarrow O_p \longrightarrow \Sigma \longrightarrow \text{status/regime},$$

where each arrow is explicitly implemented in the chamber engine.

13.5 Finite-State Structure and Its Implications

Combining the piecewise-constant law structure (Section 12) with the finite alphabet result yields a strong characterization of Axis VI operator families.

Remark 12 (Finite-state structural machine). *Because the signature alphabet \mathcal{S} is finite, the operator family behaves as a finite-state structural machine: the sweep can visit only finitely many distinct law states, and each transition between states is triggered by the parameter path meeting the admissibility boundary \mathcal{C} . Even if the parameter sweep were extended indefinitely, no new law types can appear once the finite alphabet has been exhausted. Re-entries into previously visited states are permitted; genuinely new structural laws are not.*

This has a direct consequence for the law-detection mechanism of Section 11. The mechanism guarantees that laws can be identified as stability plateaus; the finite-alphabet result guarantees that the total inventory of detectable laws is bounded. A single operator family over any compact parameter interval $P = [a, b]$ can certify at most $|\mathcal{S}|$ distinct structural laws—for seismology at most $n!$ ordering types and for cosmology at most $m!$ spectral ordering types, where n and m are the number of stations and bins respectively.

Remark 13 (Alignment with the LI–LV arc). *The finite-state interpretation is consistent with the channel factorization established in the LI–LV arc. Channel separation means that the reachable signature space factors into independent channel components; the number of joint orderings across channels is bounded by the product of the per-channel alphabet sizes. Finite law count is therefore a consequence of channel factorization combined with the discrete nature of the signature extraction map.*

14 Operator Sweeps as a Structural Microscope

14.1 Resolution Interpretation

The Axis VI chambers implement controlled operator sweeps that may be interpreted as a resolution scan of the underlying representation. In the seismic chambers the parameter is the smoothing window w , while in the cosmology chambers it is the harmonic truncation level L . Both parameters act as coarse-graining controls.

For a fixed baseline input x_0 , each chamber evaluates the induced signature field

$$F(p) = \Sigma(O_p(x_0)),$$

where p denotes either w or L depending on the domain. The signature is operationally represented in the chamber output by ranking structure (seismology) or spectral ordering (cosmology).

The admissibility invariant implies that the parameter sweep decomposes into connected stability bands in which the signature remains unchanged. These bands correspond to regions where the chamber status remains stable (e.g. repeated `status="ok"` or `primary_falsifier_pass=true`). Structural transitions occur only at discrete parameter values where boundary activation is observed.

14.2 Focus Gauge and Chamber Diagnostics

The chamber diagnostics provide empirical proxies for the distance to the admissibility boundary. The margin proxy $\hat{\Delta}(p)$ appears as the field `sigma_P` (or `sigmaP`) in the CMB chambers, while the vulnerability budget $\hat{B}(p)$ corresponds to the exported field `nu`. The difference

$$\hat{E}(p) = \hat{\Delta}(p) - \hat{B}(p)$$

therefore measures the effective interior distance from the boundary.

Deep interior regimes ($\widehat{E}(p) \gg 0$) correspond to stable resolution bands in which the extracted structure persists across operator perturbations: the microscope is “in focus.” Near-boundary regimes ($\widehat{E}(p) \approx 0$) correspond to boundary activations where the structural signature becomes sensitive to the operator scale: the microscope is “at a resolution threshold.”

14.3 Microscope Guarantee

In this sense the chamber sweeps function as a structural microscope: by varying the coarse-graining parameter and monitoring admissibility diagnostics, the system reveals which observed structures persist across resolution and which depend on a particular representational scale.

The admissibility invariant is the guarantee underlying this procedure. Each stability interval I_i is a “resolution band” within which the same structural description is visible; the critical set \mathcal{C} is the discrete set of “resolution thresholds” where what is seen can change. The energy functional $E(p) = d_Y(F(p), C)$ is the focus metric: large E means the structure is robustly visible; small E means the system is at a resolution threshold.

14.4 Hierarchies of Invariants

Because the operator family admits a coarse-graining composition law (Section 7), repeating the microscope procedure at different base resolutions can reveal hierarchies of invariants:

- coarse invariants visible at low resolution (large p),
- finer invariants that only stabilize after passing certain thresholds (intermediate p),
- transitions where the effective description changes (values in \mathcal{C}).

This is the mathematical meaning of hierarchical lawhood, and it matches the “hierarchical non-isometry under operator lift” established in the LI–LV arc: the structural object remains the same entity while its geometric description changes as the resolution is varied.

15 Empirical Projection of the Invariant

The Axis VI experiments demonstrate that the same geometry arises in real domains.

Seismology

The operator parameter is the smoothing radius applied to displacement fields. The structural signature is the ranking of station displacements.

Cosmology

The operator parameter is the harmonic truncation level ℓ_{\max} . The signature is the ordering structure of spectral bins.

In both cases the parameter manifold exhibits:

- stable structural intervals,
- discrete transition strata,

- boundary activation without structural collapse.

The cross-domain contrast is consistent with the phase-diagram picture developed above: the two operator families share the same stratification type but occupy different positions on the boundary-contact intensity axis, with seismology exhibiting low BCI and cosmology high BCI.

16 The Three-Layer Symmetry of the Manuscript

16.1 A Hidden Structural Decomposition

When the manuscript is read as a whole rather than section by section, a clean symmetry becomes visible. The paper does not merely accumulate results; it organizes itself into three conceptual strata that mirror one another and, as we shall show, recapitulate the internal structure of the LI–LV chamber arc.

The three layers are as follows.

Layer I: Structural geometry. The foundational layer defines the substrate geometry itself. Its core objects are the operator family $O : P \rightarrow \text{End}(X)$, the induced signature field $F(p) = \Sigma(O_p(x_0))$, and the degeneracy set $C \subset Y$. The key result is the stratification theorem

$$P \setminus C = \bigsqcup_i I_i,$$

which is a purely topological statement: it asserts the existence of connected stability components separated by a locally discrete critical set, with no metric information required.

Layer II: Energy geometry. The second layer introduces quantitative geometry on the same structure. Its objects are the distance-to-degeneracy functional $E(p) = d_Y(F(p), C)$, the empirical proxy $\hat{E}(p) = \hat{\Delta}(p) - \hat{B}(p)$, and the polyhedral energy model

$$\hat{E}(p) \approx \min_{j \in J} \{a_j p + b_j\}.$$

This layer converts the abstract stratification into a measurable scalar field. The topology of Layer I is preserved; what is added is a distance function that quantifies how far each point lies from the critical set.

Layer III: Operational geometry. The third layer explains how the geometric structure of Layer II is accessed experimentally. Its objects are the coarse-graining semigroups (smoothing and harmonic truncation), the chamber parameter sweeps (window w in seismology, harmonic cutoff L in cosmology), and the exported diagnostics (`sigma_P`, `nu`, `status`, `primary_falsifier_pass`). The energy $\hat{E}(p)$ is computed from these fields directly.

16.2 The Triple Correspondence

The three layers stand in a precise vertical correspondence:

Layer	Concept	Mathematical object
I	Structural invariant	Stratification $P \setminus C = \bigsqcup_i I_i$
II	Energy geometry	$E(p) = d_Y(F(p), C)$
III	Empirical probe	Operator sweep, chamber exports

The downward arrow of this correspondence reads:

$$\text{topology} \longrightarrow \text{geometry} \longrightarrow \text{measurement}.$$

Each layer is a different representation of the same underlying invariant: the admissibility structure of the operator manifold.

16.3 Correspondence with the LI–LV Arc

The same three-step pattern appears in the LI–LV chamber arc, where the results distribute across the same strata:

Chamber arc result	Role in triple correspondence
Factorization inevitability of admissibility channels	Structural layer
Robustness of channel separation under perturbation	Energy layer
Hierarchical non-isometry under operator lift	Operational layer

The manuscript therefore recapitulates the LI–LV arc in theoretical form: factorization maps to the stratification theorem, robustness maps to the stability of $E(p)$ away from zero, and non-isometry maps to the domain-dependent distortion of the energy profile under different semigroup families.

16.4 The Closed Loop

The triple correspondence closes a methodological loop that is relatively rare in foundational frameworks:

$$\text{abstract theory} \longrightarrow \text{quantitative invariant} \longrightarrow \text{empirical measurement} \longrightarrow \text{return to theory}.$$

The return path is the law-detection mechanism of Section 11: empirical stability bands, once identified in chamber exports, are reinterpreted as interior admissibility regions in the abstract stratification. The measurement outcome feeds back into the theoretical layer as a certification of the invariant.

16.5 Fiber Bundle Interpretation

The triple correspondence suggests a further geometric reading. The three objects

$$C \subset Y \longleftarrow F \longleftarrow P$$

form a nested structure: parameter space P maps via F into signature space Y , which contains the degeneracy boundary C as a distinguished subset. The energy functional

$$E(p) = d_Y(F(p), C)$$

measures the distance from $F(p)$ to the boundary fiber C .

This is structurally analogous to a fiber bundle picture in which

- P is the base space (parameter manifold),
- Y is the total space carrying the signature,

- $C \subset Y$ is the boundary fiber, and
- E is the distance-to-fiber function on the total space.

In this reading, the stability intervals I_i are the pre-images under F of the complement of C in Y , and the energy functional is an intrinsic geometric quantity associated with the fibration. Sections of the bundle correspond to choices of structural signature at each parameter value, and the admissibility condition is the statement that the section does not meet the boundary fiber.

This interpretation is not required by any of the preceding results, but the mathematics already exhibits the relevant structure. It suggests that the UNNS admissibility framework may admit a natural formulation in the language of geometric mechanics or differential topology, where the triple correspondence becomes a single coordinate-free statement about distance to a boundary stratum in a fibered space.

Remark 14. *The summary sentence that captures all three layers simultaneously is: The UNNS admissibility invariant appears simultaneously as a topological stratification of operator families, as a geometric energy functional measuring distance to degeneracy, and as an empirical phase structure revealed by chamber operator sweeps.*

17 Conclusion

The analysis developed above shows that admissibility in the *Unbounded Nested Number Sequences* (UNNS) substrate induces a natural phase geometry on operator families. Under minimal regularity assumptions (bounded perturbation envelope, Lipschitz signature field, and positive separation from degeneracy), the parameter manifold of an operator family decomposes into connected stability regions separated by a locally discrete critical set where structural transitions may occur. This stratified geometry appears internally in the LI–LV structural arc, theoretically in the Structural Lawhood formulation, and empirically in the Axis VI operator sweeps.

The geometric consequences of this invariant extend in several directions. The empirical energy profile $\widehat{E}(p)$ is consistent with a polyhedral (tropical) structure in which active-set switches generate the critical set. The semigroup structure of the two Axis VI operator families—smoothing forms an additive semigroup and harmonic truncation forms a projection semigroup—yields a renormalization-flow analogy in which stability intervals are fixed-signature regimes under scale operations. The degeneracy locus induces a codimension-one admissibility boundary in operator space whose near-critical and interior sampling regimes explain the contrasting stratification densities of cosmology and seismology. Operator families can be classified by a phase diagram whose discrete axis is stratification type and whose continuous axis is boundary-contact intensity; the categorical form of this classification identifies coarse-graining-equivalent families as phase-equivalent objects.

The convergence of these observations indicates that admissibility geometry functions as a substrate-level structural principle governing operator perturbations across domains.

The relationship between the three components of the UNNS program is:

1. The LI–LV arc establishes admissibility geometry within the substrate.
2. The Structural Lawhood manuscript provides a framework-neutral formulation of this geometry.
3. The Axis VI experiments demonstrate that the same structure appears in empirical domains and locate two operator families on the operator-family phase diagram.

Together these results indicate that admissibility geometry is not merely an internal property of recursive mechanism systems but a general structural principle governing operator perturbations. Axis VI can therefore be read as an empirical test that coarse-graining operator families induce fixed-signature regimes separated by critical scales—a renormalization-flow phase geometry governed by admissibility distance to degeneracy—and that distinct physical domains implementing different microscopic dynamics can nonetheless share the same coarse-grained phase structure.